The resonance line now cuts the $P - I$ plane at 45°, and the extrinsic diffusion coefficient increases to

$$D_p = D_{\perp E} \cot^2 \psi. \tag{6.3.35}$$

Considering P as a parameter, and using (6.3.30), we find the component of the oscillation center diffusion along I to be $D_r = D_p$. Comparing (6.3.35) and (6.3.4)

$$D_r = D^{\text{osc}} \cos^2 \psi. \tag{6.3.36}$$

We note from Fig. 6.18a that D_r is the diffusion coefficient for the oscillation center, projected along the libration direction. This shows the corresondence between the point of view in Section 6.3a and in this subsection.

For many degrees of freedom, the corresponding transformations can also be made, with the general transformation procedure having been described under the rubric *orthogonal metrics* by Chirikov (1979).

6.4. Diffusion in Toroidal Magnetic Fields

An example of considerable importance for plasma confinement, which exhibits both intrinsic and extrinsic diffusion, is that of particle motion in toroidal magnetic fields. The diffusion can be either of the magnetic field lines themselves, or of particles moving across the field lines. Of particular interest is the case of particles diffusing across magnetic field lines in the presence of both a wave field and extrinsic stochasticity (particle collisions or noisy fields). For this case, depending on the relation between the wave field, and the particle motion, there can be either diffusion in a single action, governed by the restrictions discussed in Section 5.6b, or diffusion in two actions, leading to the resonance streaming of Section 6.3. In Section 6.4a we consider the basic processes of resonance island formation in toroidal magnetic fields. In Section 6.4b we discuss qualitatively the effect of particle drifts and the resultant extrinsic diffusion. We contrast the situation in which the resonant island centers are fixed with the case in which the island centers diffuse. In Section 6.4c we treat an example of the latter case, illustrating the theory developed in Section 6.3b. In Section 6.4d we introduce the subject of self-consistent motion, where the field driving the particle motion depends in part on the particle motion itself.

6.4a. Magnetic Islands

Magnetic Field Configurations. The simplest toroidal magnetic field configuration is that produced by a long current-carrying conductor. (Here the torus is in configuration space, rather than phase space.) This magnetic field

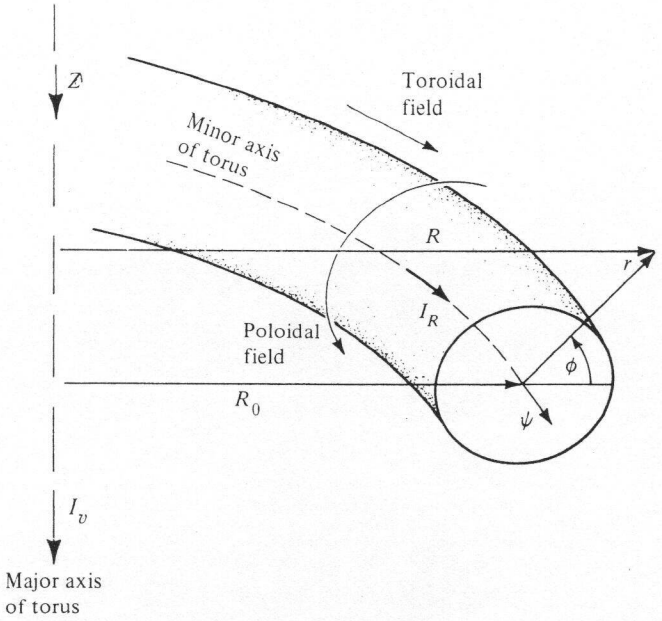

Figure 6.19. Toroidal magnetic field configuration.

does not confine particles, due to drifts across field lines. However, the addition of a toroidal current gives rise to a second field component, known as a poloidal field, at right angles to the toroidal field. This results in a helical field pattern around the torus as shown in Fig. 6.19. The field lines are similar in structure to the trajectories for the two-dimensional oscillator, as given in Fig. 3.1a. The complete conditions for the confinement and stability of a plasma, which has collective modes of behavior, will not be considered here. These conditions have led to a variety of current configurations, including a rigid toroidal current-carrying conductor at the minor axis $r = 0$, together with a vertical field (the levitron), an external helical conductor at $r = a$ around a physical torus (the stellarator), and a toroidal plasma current centered on the minor axis (the tokamak).

For these configurations the equations of the magnetic field lines can be put in Hamiltonian form (see, e.g., Morozov and Solov'ev, 1966; Rosenbluth *et al.*, 1966; and Freis *et al.*, 1973). For configurations that have azimuthal symmetry $\partial/\partial\psi \equiv 0$ (the tokamak and levitron), the equations have the form of a one-degree-of-freedom nonlinear oscillator, with the invariant being the flux enclosed within a magnetic surface (see below for definitions of these quantities). The breaking of this azimuthal symmetry effectively introduces an explicit dependence of the "timelike" variable ψ into the Hamiltonian, and thus all the consequent complexity of a two-degree-of-freedom system.

This includes the breakup of the magnetic surfaces into magnetic islands with stochastic separatrix layers and, depending on the perturbation strength, either local or global stochastic wandering of field lines.

Magnetic Surfaces. The equations of the field line are defined in (r, ϕ, ψ) coordinates by

$$\frac{dr}{B_r} = \frac{r\,d\phi}{B_\phi} = \frac{R\,d\psi}{B_\psi}, \tag{6.4.1}$$

where r and $R = R_0 + r\cos\phi$ are the local minor and major radii of the field line (see Fig. 6.19), and B_r, B_ϕ, and B_ψ are the three components of the magnetic field. In these coordinates, B_r and B_ϕ are poloidal field components and B_ψ is the toroidal field component. For a tokamak with $B_\psi = B_0$ at $R = R_0$, the field can be approximated by (Solov'ev and Shafranov, 1970)

$$\boldsymbol{B} = \left(0, \frac{\bar{B}_\phi(r)}{h_s}, \frac{B_0}{h_s}\right), \tag{6.4.2}$$

where $h_s = 1 + (r/R_0)\cos\phi$ gives the field strength variation from the outside to the inside of the torus, and contains all the ϕ variation. In the levitron a vertical field is required for the plasma equilibrium. This introduces an additional ϕ dependence that is much stronger than the toroidally produced variation. Neglecting the latter, $\boldsymbol{B}$ can be written as

$$\boldsymbol{B} = \left(B_v \sin\phi, \frac{B_0}{\beta r} + B_v\cos\phi, B_0\right), \tag{6.4.3}$$

where B_v is the vertical field (assumed upward in Fig. 6.19), and β relates the ring current to the vertical current, $\beta = I_v/I_R R_0$. The vertical field weakens the poloidal field on the inside of the torus, giving a poloidal field null ($B_\phi = 0$) at $\phi = \pi$ for $r = B_0/\beta B_v$. If the field given by (6.4.2) or (6.4.3) is substituted into (6.4.1), the field lines trace out a set of concentric surfaces having toroidal symmetry and nested about the minor axis of the torus. These are called magnetic surfaces. For the levitron field, a set of magnetic surfaces in a ψ = constant plane is shown in Fig. 6.20. Note the presence of a magnetic surface with a separatrix, the x-point corresponding to the poloidal field null.

As we shall see, the only quantity of importance in characterizing an unperturbed magnetic surface is the value of the rotational transform (angular frequency of ϕ per passage around the major axis)

$$\iota = \int_0^{2\pi} \frac{d\phi}{d\psi}\,d\psi = 2\pi\alpha, \tag{6.4.4}$$

where α is the rotation number, as previously defined. For the tokamak, h_s tends to be near unity, with a small oscillatory component. We can obtain an unperturbed Hamiltonian by introducing the canonical action variable

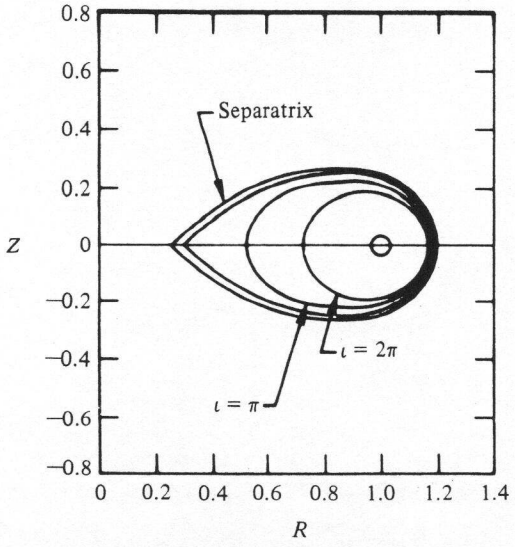

Figure 6.20. Magnetic flux surfaces for the levitron projected onto a plane $\psi = \text{const.}$; $R_0 = 1$ (after Freis *et al.*, 1973).

$\zeta = r^2/2$, and setting $h_s = 1$. The equations of motion (6.4.1) are then

$$\frac{d\zeta}{d\psi} = 0, \qquad \frac{d\phi}{d\psi} = \frac{\iota(\zeta)}{2\pi},$$

which can be derived from the Hamiltonian

$$H_0(\zeta) = \frac{1}{2\pi}\int_0^{\zeta} \iota(\zeta)\, d\zeta = \text{const.}, \tag{6.4.5}$$

which is clearly in action-angle form. Similarly, for the levitron field, from (6.4.3), setting $B_0 = 1$ for convenience,

$$\begin{aligned} \frac{d\zeta}{dz} &= B_v\sqrt{2\zeta}\sin\phi, \\ \frac{d\phi}{dz} &= \frac{1}{2\beta\zeta} + \frac{B_v}{\sqrt{2\zeta}}\cos\phi, \end{aligned} \tag{6.4.6}$$

where $z = \psi/2\pi$. Equations (6.4.6) can be derived from a Hamiltonian

$$H = -\frac{1}{\beta}\left[\ln\left(\frac{8}{\sqrt{2\zeta}}\right) - 2\right] + B_v\sqrt{2\zeta}\cos\phi.$$

For this case, before we consider the perturbation, we must transform to

action-angle variables, as in Section 1.2,

$$J = \frac{1}{2\pi}\int_0^{2\pi} \zeta \, d\phi, \tag{6.4.7a}$$

$$\bar{\phi} = \frac{\partial S(J, \phi)}{\partial J}, \tag{6.4.7b}$$

where S is the generating function. Using perturbation theory as in Section 2.2 or 2.5 to second-order,

$$H_0 = \frac{1}{\beta}\ln\left(\frac{8}{\sqrt{2J}} - 2\right) - 2B_v^2\beta J - \tfrac{3}{2}B_v^4\beta^3 J^2 \tag{6.4.7c}$$

with a rotational transform $\iota = dH_0/dJ$. A given value of ι specifies a particular magnetic surface for the unperturbed system. We emphasize that with azimuthal (ψ) symmetry, the Hamiltonian for the magnetic field lines describes a system with a single degree of freedom, and therefore the field line trajectory is completely integrable.

From the above examples it is apparent that two-dimensional magnetic fields have a Hamiltonian form. This follows from the divergence-free property of the field as can be seen explicitly in x, y, z coordinates with no z-variation

$$\frac{\partial B_x}{\partial x} + \frac{\partial B_y}{\partial y} = 0. \tag{6.4.8}$$

The field line equations can then be written in Hamiltonian form

$$\frac{dx}{dz} = \frac{B_x}{B_z} = -\frac{\partial H}{\partial y}, \qquad \frac{dy}{dz} = \frac{B_y}{B_z} = \frac{\partial H}{\partial x},$$

which satisfies (6.4.8). For field variation in three dimensions there is still a Hamiltonian form for the field line equations, but the representation is not as direct (Boozer, 1983, 1984).

Magnetic Islands. As a model for the magnetic field perturbation, we consider an additional term in the Hamiltonian

$$H = H_0(J) + \epsilon H_1(J, \bar{\phi}, \psi) \tag{6.4.9}$$

and expanding about the unperturbed orbits, $J = J_0 + \Delta J$ and $\bar{\phi} = (\iota/2\pi)\psi + \Delta\bar{\phi}$ (where $J_0 = \zeta_0$ for the tokamak approximation), we obtain a pair of perturbation equations of the form

$$\begin{aligned} \frac{d\Delta J}{d\psi} &= \epsilon \sum_{m,n} A_{mn}\cos(m\bar{\phi} - n\psi + \chi_{mn}), \\ \frac{d\Delta\bar{\phi}}{d\psi} &= \frac{1}{2\pi}\frac{d\iota}{\partial J}\Delta J, \end{aligned} \tag{6.4.10}$$

where the A_{mn} are the Fourier components of $\partial H_1/\partial\phi$. Choosing unperturbed magnetic surfaces (or J_0) such that the rotational transform gives a resonance between the poloidal and toroidal field line motion

$$m\bar{\phi} - n\psi = 2\pi k, \qquad k \text{ integer},$$

than a transformation to a rotating frame, as in Section 2.4,

$$\hat{\phi} = m\bar{\phi} - n\psi$$

gives the Hamiltonian for the perturbed motion

$$\hat{H} = \frac{m^2}{2\pi}\frac{d\iota}{dJ}\frac{\Delta\hat{J}^2}{2} + \epsilon A_{mn}\cos\hat{\phi}, \tag{6.4.11}$$

where $\Delta\hat{J} = \Delta J/m$. The half-width of the island separatrix is then, from (2.4.31),

$$\Delta\hat{J}_{\max} = \frac{2}{m}\left|\frac{\epsilon A_{mn}}{(1/2\pi)(d\iota/dJ)}\right|^{1/2}. \tag{6.4.12}$$

As an illustration of island formation, a ψ-dependent perturbation was introduced into the levitron magnetic field by tilting the ring current (Freis *et al.*, 1973). Using (6.4.12) with the known value of A_{mn}, they compared the perturbation result with exact numerical integration of the field line equations (6.4.1). The agreement for the $m = n = 1$ island ($\iota = 2\pi$), was excellent, provided the perturbation did not exceed the threshold for global stochasticity. For larger perturbation, the break-up into chains of secondary islands was observed, as expected from the theory of Sections 2.4 and 4.3. In Fig. 6.21a the theoretical (solid lines) and numerical (dots) island widths are given showing the island forming on the inside of the $\iota = 2\pi$ magnetic surface. The banana shape of the island in physical space is evident. The local rotation number around the island is $\alpha = 1/5.6$, and second-order island structure is not in evidence. In Fig. 6.21b the perturbation amplitude (ring tilt) has been increased until the local rotation number $\alpha = \frac{1}{4}$ (the island number nearest the elliptic singular point is 4). The theoretically predicted island has broken up into four unstable second-order island clumps, and the long-time fieldline motion is, in fact, stochastic. A second-order island calculation, as in Section 2.4b, reveals that the $\alpha = \frac{1}{4}$ and $\alpha = \frac{1}{5}$ islands overlap, leading to the observed stochasticity.

The same form of the island perturbation was obtained for a helical external current by Rosenbluth *et al.* (1966) and Filonenko *et al.* (1967); for general current perturbations in tokamaks by Rechester and Stix (1976) and Finn (1977); and for the $m = n = 1$ mode helical current by Lichtenberg (1984). For all of these cases, the perturbation acts directly on the magnetic surfaces and breaks the resonant surfaces into finite width islands. For the $m = n = 1$ mode, the assumed single helicity perturbation emphasizes the interaction that couples the helical mode to the $m = 1$, $n = 0$ toroidal

Figure 6.21. Comparison of theoretical and numerical (○) results for the $\iota = 2\pi$ island at two values of ring tilt perturbation (a) $\delta = 0.25°$; (b) $\delta = 0.5°$ (after Freis *et al.*, 1973).

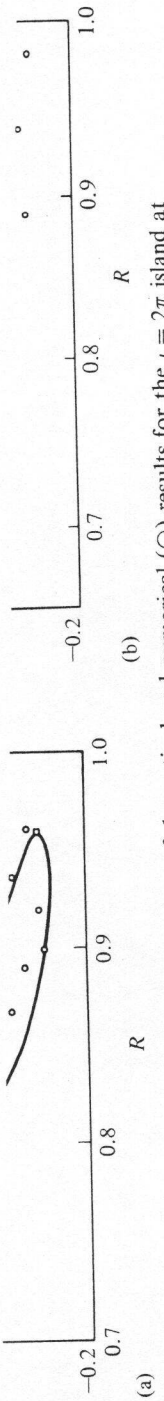

Figure 6.21. Comparison of theoretical and numerical (○) results for the $\iota = 2\pi$ island at two values of ring tilt perturbation (a) $\delta = 0.25°$; (b) $\delta = 0.5°$ (after Freis *et al.*, 1973).

symmetry which generates second-order islands. The width of the stochastic region surrounding the main island, due to overlap of second-order islands, was compared to the numerically calculated stochastic width giving excellent agreement. In these problems it is assumed that the charged particles in the system follow the field lines exactly, and thus the finite Larmor radius of the particles plays no role. Since we are considering a time-independent Hamiltonian in two degrees of freedom, the intrinsic diffusion resulting from island overlap is that derived in Chapter 5, and diffusion along resonances is absent.

For the problem of externally applied helical fields, using the stellarator concept to achieve a plasma equilibrium, the applied fields generate magnetic islands that are particularly severe near the outside of the plasma volume, as analyzed originally by Rosenbluth *et al.* (1966) and Filonenko *et al.* (1967). Since these fields are somewhat under the control of the machine designer, the question can be asked whether the fields can be designed to increase the plasma volume having good flux surfaces; i.e., small islands and little stochasticity. The obvious answer is to minimize those harmonic components in the field that supply the principal contributions to the most harmful edge islands. Because of the complexity of stellarator fields, and the lack of clear identification of the most destructive islands, the procedures can be quite complicated. Two related approaches have been developed to do this: Cary (1982) varied components until the adjacent edge island pairs did not overlap (good KAM magnetic surfaces exist); and Hanson and Cary (1986) used a simpler procedure of examining the island residues. These results showed that the plasma volume contained by good magnetic surfaces could be increased by almost a factor of two.

6.4b. Drift Surfaces and Diffusion in Static Fields

Drift Surfaces. Finite temperature charged particles gyrating around magnetic field lines in nonuniform magnetic or electric fields are not completely tied to the field lines, but drift slowly across them. Fourier components of the nonuniform field variation having the major radius periodicity can resonate with Fourier components of the minor radius periodicity, leading to drift surface islands. The drift equations for particle motion in a current-free field are given by (see, e.g., Schmidt, 1979, Section 2.2)

$$\boldsymbol{v}_D = \frac{d\boldsymbol{r}}{dt} = \frac{\boldsymbol{F} \times \boldsymbol{B}}{eB^2} + v_{\|} \frac{\boldsymbol{B}}{B}, \tag{6.4.13a}$$

$$\frac{dv_{\|}}{dt} = -\frac{e}{M} \frac{\partial \Phi}{\partial s} - \frac{\mu}{M} \frac{\partial B}{\partial s}, \tag{6.4.13b}$$

where e and M are the particle charge and mass,

$$\boldsymbol{F} = -\left(\mu + \frac{Mv_{\|}^2}{B}\right)\nabla B - e\nabla\Phi$$

is the force averaged over a gyro-orbit, $\mu = \frac{1}{2}Mv_{\perp}^2/B$ the magnetic moment, Φ the electric potential, $v_{\|}$ the particle velocity along the field line, s the coordinate along the field line, and $\boldsymbol{r}$ the guiding center position of the gyrating particle. In the drift approximation, μ is an adiabatic invariant and is assumed to be well conserved (see Section 2.3b). If B and Φ are not explicit functions of time, then the motion is described by a reduced Hamiltonian that is autonomous and has two degrees of freedom. In this case, the time can be eliminated in favor of s as the independent variable by using

$$\frac{d}{dt}(s) = v_{\|},$$

where $v_{\|}$ is related to the constants of the motion μ and E through the relation

$$v_{\|} = \left(\frac{2}{M}\right)^{1/2}(E - \mu B)^{1/2}, \tag{6.4.14}$$

and E is the total energy. The resulting drift motion then occurs in a system with two degrees of freedom, which is completely analogous to the magnetic field line motion described in the previous section.

Nonresonant Motion. Consider first a magnetic field gradient alone. For magnetic surfaces that have no ϕ-variation (see Fig. 6.19), $\boldsymbol{F}$ is perpendicular to the magnetic surface, and $\boldsymbol{v}_D$, as seen from (6.4.13), lies in the surface. However, for toroidal fields of the levitron or tokamak type, the lack of ϕ symmetry gives rise to radial drifts. The time scale for this drift motion is generally long compared to the time scale for motion along the field. Thus neglecting high-order resonances, the radial motion can be described by a one-dimensional autonomous Hamiltonian and is thus integrable.

There are two kinds of orbits depending on whether or not $v_{\|} \ll v_{\perp}$. For $v_{\|} \ll v_{\perp}$, particles are trapped on a field line near the outside of the torus ($\phi \approx 0$) and bounce back and forth between high field regions located on the inside of the torus. The drift motion then appears as a "banana" when projected onto a ψ = const. plane. The width of the banana Δr at $\phi = 0$ is proportional to the particle's Larmor radius ρ_L but enhanced by the ratio of the major-to-minor radii of the torus

$$\Delta r \sim \left(\frac{R}{a}\right)^{1/2}\frac{\rho_L}{\iota}. \tag{6.4.15}$$

The banana shape is similar to that seen in Fig. 6.21a except that it is thinner

(because of the ρ_L proportionality) and is on the outside of the torus. These banana orbits exist on any magnetic surface for trapped particles (see Solov'ev and Shafranov, 1970 for a complete discussion), and therefore do not depend on resonances between the ϕ and ψ motion.

For the case of passing particles, the particles drift on a surface that is similar in shape to and within a distance $\pm\rho_L/\iota$ of the magnetic surface. The orbits are just slightly perturbed versions of the magnetic surfaces.

Drift Islands. If we now allow B and Φ to vary in both ϕ and ψ, passing particles experience resonances between the ϕ and ψ motion that lead to drift islands. For magnetic gradients, because of the ρ_L dependence, these drift islands are small compared to the magnetic islands arising from the same perturbation. If a static electric field exists, such as a drift wave, with Fourier expansion

$$\Phi = \sum \Phi_{mn} \exp[i(m\phi - n\psi)],$$

then drift islands are formed due to resonance between the ϕ and ψ motion. The island widths are proportional to the potential and thus the drift islands are formed independently of the amplitude of any magnetic islands that may exist due to field line motion. A set of equations of the form of (6.4.10) can then be obtained for the perturbed motion, with the Fourier amplitudes ϵA_{mn} proportional both to the Fourier coefficients of the potential Φ_{mn} and to the Larmor radius ρ_L. This calculation was performed by Brambilla and Lichtenberg (1973), to obtain an island half-width, analogous to (6.4.12) but measured in physical space,

$$\Delta r = 2\left(\frac{e\Phi_{mn}}{kT}\frac{R}{a}\frac{\rho_L}{d\iota/dr}\right)^{1/2}. \tag{6.4.16}$$

Here kT is the characteristic particle energy (k is Boltzmann's constant and T is the temperature).

Diffusion in Static Fields. The width of the resonant islands given by (6.4.16) may be large compared to the width of the nonresonant banana motion given by (6.4.15). Nevertheless, for static fields, the nonresonant bananas are usually more important in giving rise to extrinsically driven diffusion. The reason for this apparent contradiction is easy to see. For static potentials, the resonant drift surface islands are centered on fixed magnetic surfaces, $m\omega_\phi - n\omega_\psi = 0$. Since $\omega_\phi/\omega_\psi = d\phi/d\psi$, a function of r alone, the locations of the resonance centers are independent of $v_\parallel$ and μ. The diffusion arising from weak interparticle collisions, which causes $v_\parallel$ and μ to vary in a random manner, is therefore of the type discussed in Section 5.6b. (If the drift islands overlap, then the resulting intrinsic global stochasticity generally determines the diffusion rate; however, because of the ρ_L dependence in the island amplitude, the islands rarely overlap, and we ignore intrinsic diffusion in the

following argument.) For large but nonoverlapping islands, there is enhanced diffusion across each island width. However, the overall diffusion rate is limited to much smaller values by the nonresonant drift surfaces between islands.

In contrast, the nonresonant banana orbits of the trapped particles exist on any magnetic surface and are therefore not inhibited in this manner. Collisional changes of $v_\parallel$ and μ scatter the particles from trapped to passing orbits. Each such scatter either transfers the average radial particle position from its instantaneous position on a passing orbit to the center of the banana on a trapped orbit, or conversely. Depending on the collisionality, three distinct types of behavior are observed when banana orbits are present.

1. For low collisionality, the particles step on the average a distance of a banana width in the time it takes for $v_\parallel$ to diffuse across a resonance width. Since this time is proportional to the collision time, the diffusion rate is proportional to the collision frequency.
2. For intermediate collisionality, a resonant particle does not execute a full banana oscillation before it is detrapped. The step size is thus reduced to a fraction of a banana width. However nonresonant particles near the separatrix now also have oscillations of order this step size, and thus contribute to the overall diffusion. Furthermore the effective resonance width is increased, and thus the time to diffuse across the resonance region is also increased. Including the three effects of increased diffusion time, increased fraction of particles, and decreased step size, the result is a diffusion coefficient independent of collision frequency. This case is therefore usually called the plateau regime.
3. For high collisionality, a fluid model must be used to calculate the diffusion. The resulting value of Δr, the step size in the diffusion coefficient, is enhanced by a factor of $1/\alpha$ [see (6.4.4)] over the gyroradius, and the consequent diffusion, known as "Pfirsch-Schlüter" diffusion, is again proportional to collision frequency.

The characteristic step sizes in all cases are proportional to the Larmor radius $\rho_L = v_T/\Omega$; thus the diffusion coefficient D has the classical scaling $D \propto \rho_L^2 \propto 1/B^2$ and is therefore known as *neoclassical diffusion.* The reader interested in detailed calculations of this process is referred to a review by Galeev and Sagdeev (1979). As mentioned in Section 6.3a, these three regimes also exist in resonance streaming problems.

6.4c. Time-Varying Fields

In this section we consider a problem related to neoclassical diffusion in that the perturbed orbits are banana shaped and can exist on any magnetic surface. However, the perturbation to be treated is resonant, and thus the "bananas" are really islands whose widths can be strongly enhanced over

those for neoclassical diffusion. The reason that these islands can exist on any magnetic surface is the inclusion of a time variation in the potential. This introduces another degree of freedom into the perturbed Hamiltonian such that the energy E is no longer conserved. Thus one cannot eliminate $v_\parallel$ from the motion using (6.4.14), and the resonance condition becomes

$$m\omega_\phi(r, v_\parallel) + n\omega_\psi(r, v_\parallel) + l\omega = 0,$$

where ω is the frequency of the potential variation. This condition yields for the location of a resonance center (with fixed m, n, and l)

$$r = r(v_\parallel, \omega).$$

If there is continuous extrinsic diffusion of $v_\parallel$, then the resonance center will continuously diffuse in r. The diffusion is thus an example of the resonance streaming developed in Section 6.3 and can, in particular, be transformed directly into the mapping form described in Section 6.3b.

If the potential arises from a field which is time varying, then the phase of the potential for a particle position r is given by

$$\theta = \boldsymbol{k}\cdot\boldsymbol{r} - \omega t, \tag{6.4.17}$$

where $\boldsymbol{k}$ is the wave vector and ω the wave frequency. Within the drift approximation the particle velocity is parallel to the field lines, i.e., drift velocities are assumed slow compared to particle velocities. The rate of change of phase is therefore given by

$$\frac{d\theta}{dt} = k_\parallel(\boldsymbol{r})v_\parallel - \omega, \tag{6.4.18}$$

where $k_\parallel$ is the wavenumber parallel to the magnetic field. As described above, the parallel particle velocity is no longer ignorable, and the resonance center diffuses as $v_\parallel$ diffuses. This problem has been treated by Gell *et al.* (1975) and in more detail by Nevins *et al.* (1979).

Construction of the Mapping Equations. We simplify the magnetic field geometry by using rectangular coordinates with x corresponding to r. The coordinate system used is shown in Fig. 6.22. Here $\boldsymbol{k} = k_0\hat{\boldsymbol{y}}$ is a fixed wavevector, and $\boldsymbol{B}(x)$ lies in the $y - z$ plane with $B_y = 0$ at $x = 0$. We define the shear length L_S by

$$B_y(x) = B\frac{x}{L_S},$$

where for a torus $L_S^{-1} = (R/a)(d\iota/dr)$. The component of $\boldsymbol{k}$ parallel to $\boldsymbol{B}$ is then given by

$$k_\parallel(x) = k_\perp\frac{x}{L_S}, \tag{6.4.19}$$

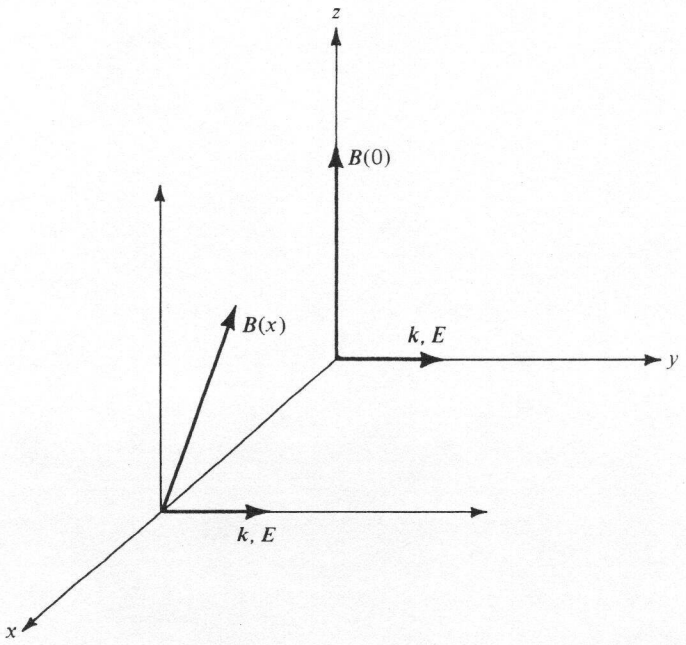

Figure 6.22. The configuration of the model for calculation of resonance drift island diffusion.

where to first order we set $k_0 = k_\perp$. Taking the potential of the wave to be of the form

$$\Phi = \Phi_0 \cos\theta, \tag{6.4.20}$$

then (6.4.13a) and (6.4.13b) can be written in the form

$$\frac{dx}{dt} = \frac{k_\perp}{B}\Phi_0 \sin\theta, \tag{6.4.21}$$

$$\frac{dv_\parallel}{dt} = \frac{e}{M}k_\parallel \Phi_0 \sin\theta. \tag{6.4.22}$$

Equations (6.4.21) and (6.4.22), together with (6.4.18), describe the perturbed motion in the absence of collisions. We assume that at a given $x = x_0$ resonance occurs for a velocity $v_{\parallel 0}$ such that (6.4.18) becomes

$$k_{\parallel 0} v_{\parallel 0} - \omega = 0, \tag{6.4.23}$$

where we have used the notation $k_\parallel(x_0) = k_{\parallel 0}$. At resonance, with $\theta = 0$, the particle motion is unperturbed by the potential. We follow the usual procedure of considering the perturbed motion about resonance by linearizing

$x = x_0 + \Delta x$ and $v_\parallel = v_{\parallel 0} + \Delta v_\parallel$ to obtain

$$\Delta\dot{x} = \frac{k_\perp}{B}\Phi_0 \sin\theta, \tag{6.4.24}$$

$$\Delta\dot{v}_\parallel = \frac{e}{M} k_{\parallel 0}\Phi_0 \sin\theta + \zeta, \tag{6.4.25}$$

and

$$\dot{\theta} = \frac{k_\perp}{L_S} v_{\parallel 0}\Delta x + k_{\parallel 0}\Delta v_\parallel, \tag{6.4.26}$$

where to obtain (6.4.26) we have expanded (6.4.19) about $x = x_0$ and inserted this into (6.4.18). The dots are the total time derivatives. We have further added to (6.4.25) the random velocity component ζ due to interparticle collisions, such that, for collisions alone,

$$\langle \Delta v_\parallel^2 \rangle = \frac{v_T^2}{\tau_c} t, \tag{6.4.27}$$

where v_T is the thermal velocity and τ_c is the collision time. A change in ζ changes $v_\parallel$ without changing x, and thus changes the resonance center of the perturbed motion according to (6.4.23). We must therefore transform our equations to the appropriate form to decouple the diffusive motion from the resonance motion, as illustrated in Fig. 6.18, i.e., transform Eqs. (6.4.24)–(6.4.26) to the form of (6.3.28). To do this we introduce a new variable y for which the dynamical part of (6.4.25) is eliminated. Multiplying (6.4.24) by $(e/M)\, k_{\parallel 0}(B/k_\perp)$ and subtracting this from (6.4.25), we have

$$\Delta\dot{v}_\parallel - \frac{\Omega k_{\parallel 0}}{k_\perp}\Delta\dot{x} = \zeta. \tag{6.4.28}$$

Defining y as

$$y = \Delta v_\parallel - \frac{\Omega k_{\parallel 0}}{k_\perp}\Delta x, \tag{6.4.29}$$

we have a new form of (6.4.25) for the random motion alone

$$\dot{y} = \zeta. \tag{6.4.30}$$

Solving (6.4.28) for $\Delta v_\parallel$ in terms of y and Δx and substituting into (6.4.26), we have

$$\dot{\theta} = k_{\parallel 0} y + \frac{k_{\parallel 0}^2}{k_\perp}\Omega(1 + S)\Delta x, \tag{6.4.31}$$

where S, here, is a parameter measuring the importance of the shear

$$S = \frac{k_\perp^2}{k_{\|0}^2} \frac{v_{\|0}}{L_S \Omega}. \tag{6.4.32}$$

When $S \ll 1$, shear is unimportant, and the island width is limited by the ratio of $k_\|$ to $k_\perp$ at a fixed position. When $S \gg 1$, the island width is limited by the shear. A simple scale change in the variables now transforms (6.4.24), (6.4.31), and (6.4.30) into the standard form of (6.3.28). Setting

$$I = \frac{k_{\|0}^2}{k_\perp} \Omega(1 + S)\Delta x \tag{6.4.33a}$$

and

$$P = k_{\|0} y, \tag{6.4.33b}$$

then

$$\dot{I} = K \sin\theta, \tag{6.4.34a}$$

$$\dot{\theta} = I + P, \tag{6.4.34b}$$

$$\dot{P} = \xi, \tag{6.4.34c}$$

where

$$K = k_{\|0}^2 v_T^2 (1 + S) \frac{e\Phi_0}{kT}, \tag{6.4.35a}$$

$$\xi = k_{\|0} \zeta, \tag{6.4.35b}$$

and we have defined v_T by $Mv_T^2 = kT$. The island width scales in the usual manner as $K^{1/2}$.

Diffusion Calculation. We are now in a position to calculate the resonant diffusion in I, as in Section 6.3b. Using the definition of ζ from (6.2.25) and (6.2.27) in (6.4.34c) with ξ given by (6.4.35b) we obtain

$$\langle P^2 \rangle = \frac{k_{\|0}^2 v_T^2}{\tau_c} t.$$

The diffusion coefficient is then

$$D_r = \frac{\langle I^2 \rangle}{2t} = \frac{\langle P^2 \rangle}{2t} = \tfrac{1}{2} k_{\|0}^2 v_T^2 / \tau_c. \tag{6.4.36}$$

Assuming that only resonant diffusion is important, then the diffusion, in I space, is given as in (6.3.33) by

$$\langle D \rangle = D_r f_p, \tag{6.4.37}$$

where f_p is the fraction of resonant particles. Taking the characteristic range

of $v_\parallel$ to be v_T, then the range of P, from (6.4.33), is $k_{\parallel 0} v_T$ and

$$f_p \approx \frac{K^{1/2}}{k_{\parallel 0} v_T} \tag{6.4.38}$$

giving

$$\langle D \rangle = \tfrac{1}{2} k_{\parallel 0}^2 v_T^2 (1 + S)^{1/2} \left(\frac{e\Phi_0}{kT} \right)^{1/2} \left(\frac{1}{\tau_c} \right). \tag{6.4.39}$$

In terms of the physical variable Δx, the diffusion is obtained by substituting the scaling from (6.4.32):

$$D_x = \frac{1}{2} \frac{k_\perp^2}{k_{\parallel 0}^2 (1 + S)^{3/2}} \left(\frac{e\Phi_0}{kT} \right)^{1/2} \frac{\rho_L^2}{\tau_c}. \tag{6.4.40}$$

The result in (6.4.40) has been obtained by Nevins *et al.* (1979) in a different manner in which the step length for diffusion is taken to be an island width, as in the two degrees of freedom problem, and an effective collision time is used

$$\tau_{\text{eff}} = \left(\frac{v_{\text{trap}}}{v_T} \right)^2 \tau_c, \tag{6.4.41}$$

where v_{trap} is estimated as

$$v_{\text{trap}}^2 = (1 + S) \frac{e\Phi_0}{M}.$$

However, the physical mechanism of resonance streaming is hidden in this presentation. The exact numerical value of the diffusion is not obtained from (6.4.40), because of the approximation of (6.4.38). The diffusion described by (6.4.40) has sometimes been called *pseudo-classical diffusion*, as it has the classical scaling $D_x \propto \rho_L^2/\tau_c$, but is enhanced by a coefficient that depends on the amplitude Φ_0 of a resonant perturbation.

Comparison of Analytical and Numerical Results. Nevins *et al.* (1979) compared all of the scalings of (6.4.40) with computer simulations using the exact equations of single particle motion and a Monte Carlo collision operator. The code follows typically 500 to 1000 particles to obtain good statistics. All of the scalings checked reasonably well, verifying the theory. Here we reproduce only two of these results. In Fig. 6.23 the effect of the shear parameter is studied by comparing the numerical results, labeled D^*, with the analytic formula for D_x in (6.4.40), with a parameter inserted for best fit. They find $D^* = 0.8 D_x$, which is good agreement, although there are some additional subtleties. In the limit $S \ll 1$, using a more exact transport theory derived in the absence of shear, Nevins and co-workers compare the numerical and analytic calculations of diffusion as a function of collision frequency. In Fig. 6.24, we see a plateau regime (so-called because it is

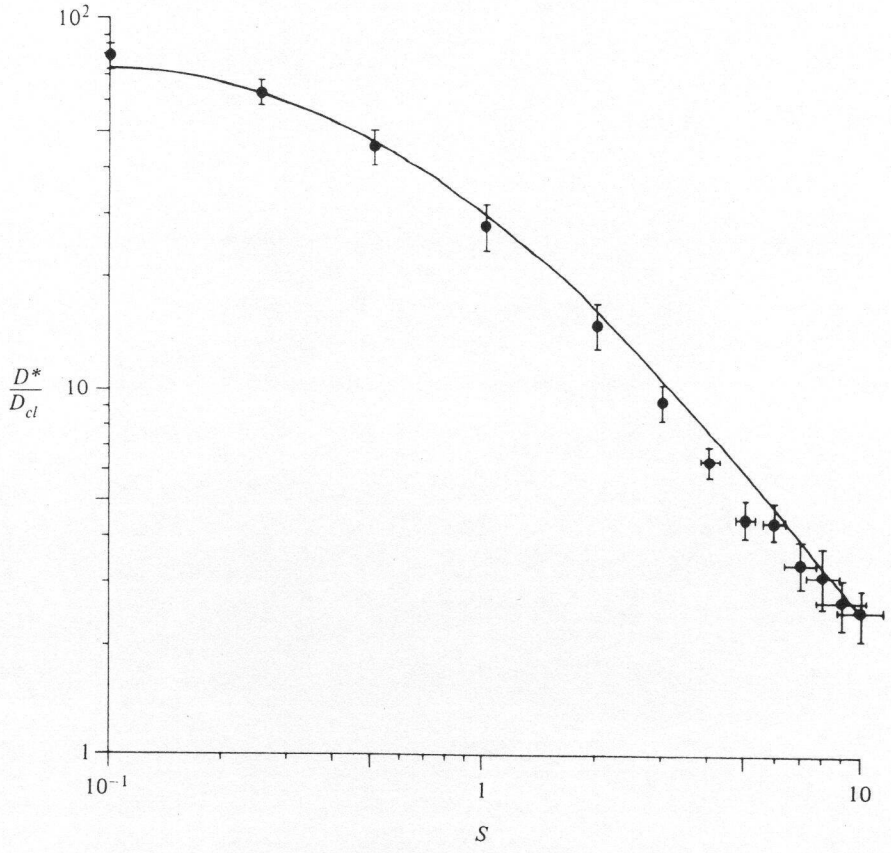

Figure 6.23. The diffusion coefficient D^* normalized to $D_{cl} = \rho_L^2/\tau_c$ versus S, showing the transition between the regimes of small and large shear. The quantities $e\Phi_0/kT$, $k_\parallel/k_\perp$, $\omega/k_{\parallel 0}v_T$, and $k_\perp\rho_L$ are held constant at 0.01, 0.03, 0.5, and 4.3×10^{-3}, respectively, while $k_\perp L_S$ is varied. The solid line is $0.8D_x$, with D_x given by (6.4.40). The horizontal error bars reflect the finite spatial resolution of the measured diffusion coefficient from the numerical simulation (after Nevins *et al.*, 1979).

independent of ν_c) and an interesting transitional regime near $\nu_{\text{eff}}/\omega_0 = 1$, where ω_0 is the frequency of the resonant oscillation of x. The solid line is the prediction of the more exact calculation for the banana regime without shear. The plateau line can be determined by making the simple assumption that for $\nu_{\text{eff}} > \omega_0$ the distance a particle drifts in x between collisions, which is the random step in the diffusion process, shortens with increasing collisionality at just the rate to keep

$$\omega_0\tau_{\text{eff}} \simeq 1. \tag{6.4.42}$$

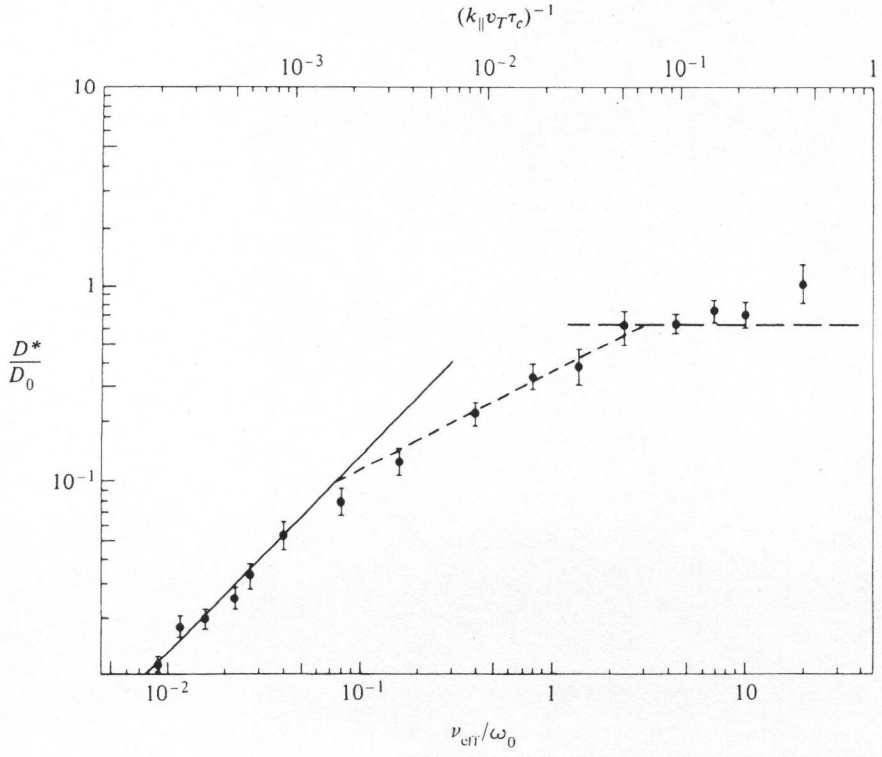

Figure 6.24. Measured values of the enhancement in the diffusion coefficient normalized to $D_0 = (k_\parallel v_T)^{-1}(k_\perp \Phi_0/B)^2$ versus the collision frequency. The solid line is given by $D^* = 1.3D_x$ with D_x given by (6.4.40). The dashed line shows the self-consistent diffusion rate given by (6.4.43). The quantities $e\Phi_0/kT$, $k_\parallel/k_\perp$, $\omega/k_{\parallel 0} v_T$ and $k_\perp \rho_L$ were held constant at 0.08, 0.2, 0, and 4.3×10^{-3}, respectively. The vertical error bars here represent fluctuations in D^* from the numerical simulations (after Nevins *et al.*, 1979).

Using (6.4.42) with $\omega_0 = K^{1/2}$ obtained from (6.4.35a) and τ_{eff} from (6.4.41) to substitute for τ_c in (6.4.40), we obtain the result for the plateau region, independent of τ_c,

$$D_{x(\text{pl})} = \frac{k_\perp^2}{k_\parallel^2} k_\parallel v_T \left(\frac{e\Phi_0}{kT}\right)^2 \rho_L^2. \tag{6.4.43}$$

The result, obtained in the limit of no shear, agrees within a small numerical factor with a kinetic theory treatment (Sagdeev and Galeev, 1969). We point out, however, that the use of (6.4.42), while reasonable, is not within the scope of the theory of oscillation center diffusion.

6.4d. The Self-Consistent Problem

Diffusion in toroidal magnetic fields illustrates a very important factor in many real problems, which has not explicitly been considered in this monograph, that of self-consistent fields; that is, the fields within which particles move may be generated in part by the collective motion of the particles themselves. In this situation the Hamiltonian that determines the dynamics is not *a priori* known. These problems have generally been attacked by numerical simulation of the complete particle and field equations, as illustrated below.

Tearing Modes and Disruptions in Tokamaks. For a tokamak device, as described in Section 6.4a, the poloidal component of the magnetic field arises from a toroidal current created by the plasma particles that are assumed to be moving on regular flux surfaces. However, the plasma can be subject to resistive tearing instabilities (e.g., White *et al.*, 1977; Carreras *et al.*, 1981), which lead to helical perturbations of the current, i.e., a current having a basic symmetry $l\phi - n\psi = \text{const.}$; l and n integers. These perturbations break the azimuthal symmetry, and the harmonics of the perturbation appear as islands on the rational surfaces. With cylindrical symmetry a single helical mode would result in a single resonant island; it would therefore not lead to island overlap and stochasticity. However, the inclusion of toroidal effects adds new major resonances. For example, a primary helically excited mode with $l = 2$, $n = 1$ excites a major two-island structure on the $\iota = \pi$ magnetic surface. The toroidal symmetry adds a significant component of a three-island structure on the $\iota = 2\pi/3$ rational surface. These rational surfaces commonly occur within the plasma of tokamaks, with consequent large magnetic islands that affect the plasma motion. In Fig. 6.25 the magnetic surface structure is shown arising from the numerical simulation of a saturated $l = 2$, $n = 1$ mode, giving rise to the $\iota = \pi$ resonant islands. The coupling through the toroidal terms also gives rise to resonant islands on the $\iota = 2\pi/3$ rational surface. Despite the large island size, little stochastic wandering of field lines was found in this case. However, if an $l = 2$, $n = 2$ helical mode is also present, then large regions of stochasticity are observed. The evolution of two such modes has been followed by numerical simulation, integrating the self-consistent field and particle equations, to obtain the result shown in Fig. 6.26. In the first frame the $\iota = \pi$ and $\iota = 2\pi/3$ islands are clearly seen. In the second frame the interaction between the current components of the $l = 2$, $n = 1$ and $l = 2$, $n = 2$ symmetries has led to stochastic wandering of most of the field lines near the $\iota = \pi$ island chain. In the third frame the interaction has spread to engulf the $\iota = 2\pi/3$ island. The resulting drastic modification of the original helical current pattern has led to the destruction of the central flux surfaces in the fourth frame. The abrupt change in the current distribution, as the islands overlap, is thought to be the cause of current disruptions in tokamaks.

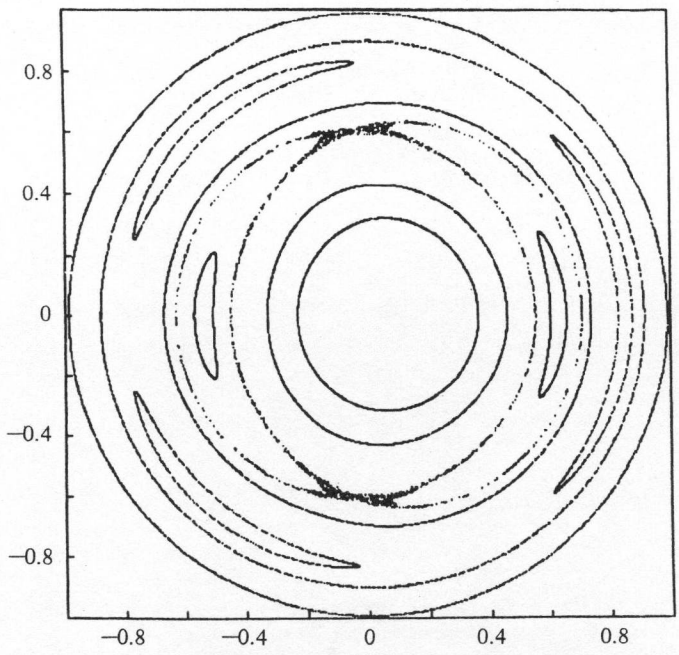

Figure 6.25. Magnetic field line plot showing a saturated 2/1 magnetic island and its 3/1 toroidal satellite (after Carreras *et al.*, 1981).

6.5. Many Degrees of Freedom

There has been considerable interest in understanding systems with a large number of degrees of freedom. The motivation, on one hand, has been concerned with the behavior of nonlinear partial differential equations, and, on the other, with the relation to the statistical mechanics of the many-body problem. In Section 6.1a we have formally considered a many-dimensional system within which a particular set of resonance surfaces can be singled out for study. A single, many-dimensional resonance has a simple resonance width, defined in the proper coordinates, and this width may be projected onto any single action of the multidimensional system. This geometric interpretation was developed further in Section 6.3, and mathematical details of the coordinate transformations to exhibit the resonance locally can be found in Chirikov (1979). From this perspective the question of a large number of degrees of freedom appears to resolve itself into the question of whether the density of important resonances, as projected onto a single action, increases faster than the widths of the resonances decrease, as the system energy is spread over more degrees of freedom. If this happens, then we would expect resonance overlap and strongly chaotic motion to occur for N degrees of freedom, as $N \to \infty$.